

# Supporting Information

## Galvanic Replacement Onto Complex Metal-Oxide Nanoparticles: Impact of Water or Other Oxidizers in the Formation of Either Fully Dense Onion-like or Multicomponent Hollow MnO<sub>x</sub>/FeO<sub>x</sub> Structures

Alberto López-Ortega<sup>†,§,\*</sup>, Alejandro G. Roca<sup>‡,\*</sup>, Pau Torruella<sup>⊥</sup>, Michelle Petrecca<sup>†</sup>, Sònia Estradé<sup>⊥</sup>, Francesca Peiró<sup>⊥</sup>, Victor Puntès<sup>‡,||,∇</sup> and Josep Nogués<sup>‡,||</sup>

<sup>†</sup>INSTM and Dipartimento di Chimica “U. Schiff”, Università degli Studi di Firenze, Via della Lastruccia 3, Sesto Fiorentino, I-50019 Firenze, Italy.

<sup>§</sup>CIC nanoGUNE, E-20018 Donostia-San Sebastian, Spain.

<sup>‡</sup>Catalan Institute of Nanoscience and Nanotechnology (ICN2), CSIC and The Barcelona Institute of Science and Technology, Campus UAB, Bellaterra, 08193 Barcelona, Spain

<sup>⊥</sup>LENS-MIND-IN2UB, Departament d’Electrònica, Universitat de Barcelona, Martí i Franquès 1, E-08028 Barcelona, Spain.

<sup>||</sup>Institució Catalana de Recerca i Estudis Avançats (ICREA), Barcelona, Spain.

<sup>∇</sup>Vall d’Hebron Institut de Recerca (VHIR), 08035 Barcelona, Spain.

e-mail: [lopezortega.alberto@gmail.com](mailto:lopezortega.alberto@gmail.com); [alejandrogroca@gmail.com](mailto:alejandrogroca@gmail.com)

### EELS Characterization

EEL spectrum images allowed elemental mapping and quantification of the Mn/Fe Core-Shell structure of samples **CS1** and **HW1**,<sup>1</sup> as shown in Figure S1a. The acquired spectra confirm the presence of MnO in sample **CS1** and Mn<sub>3</sub>O<sub>4</sub> in sample **HW1** as shown in Figure S1b,c. As can be clearly seen the ratio between Mn L<sub>3</sub> and Mn L<sub>2</sub> lines is higher for sample **CS1** than for sample **HW1** indicating that in sample **CS1** Mn has a lower oxidation state. The comparison with literature values shows that **CS1** consists of mainly MnO while **HW1** is Mn<sub>3</sub>O<sub>4</sub>.<sup>1</sup> A plot of the fine structure parameters compared to literature values is presented in Figure S1c.

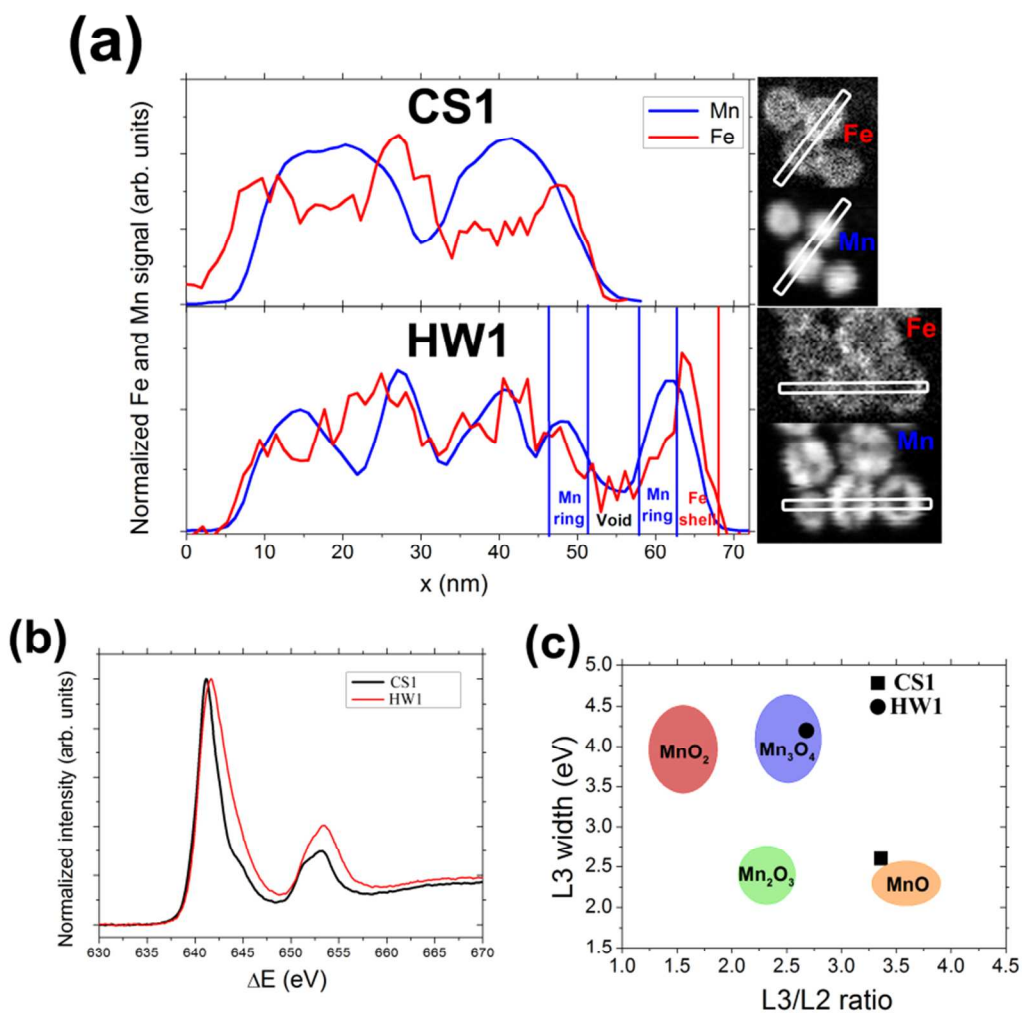


**Figure S1.** **a** Mn and Fe maps of integrated  $L_{2,3}$  edge signal for samples **HW1** and **CS1** with profiles from the highlighted areas, **b** Spectra from the Mn regions in samples **HW1** and **CS1** and **c** plot of the fine structure parameters from the spectra in **b** compared to the literature values<sup>1</sup>.

## Structural data from XRD

**Table 1.** Structural data obtained from Rietveld refinement of the XRD patterns for the different samples.

	$\text{Mn}_3\text{O}_4$			$\text{MnO}$		$\text{Fe}_3\text{O}_4$		w%
	a (nm)	c (nm)	cs (nm)	a (nm)	cs (nm)	a' (nm)	cs (nm)	
<b>S1</b>	0.578	0.913	10	0.442	13	-----	-----	65/35/0
<b>CS1</b>	0.598	0.953	11	0.453	10	0.864	4	49/18/33
<b>HW1</b>	0.576	0.928	18	-----	-----	0.839	5	0/57/43

a and c, cs, a' and w% refers to the cell parameters for the tetragonal spinel, crystalite size, cell parameter for the cubic spinel and weight fraction, respectively.

## Magnetic Properties

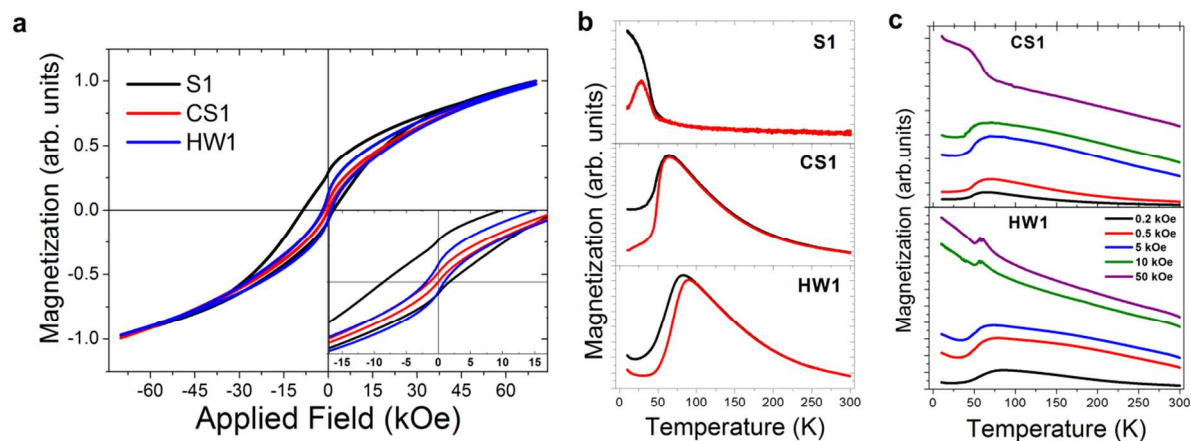


**Figure S2.** **a** Field cooled hysteresis loops at 10 K for the **S1**, **CS1** and **HW1** samples. The inset shows a magnification of the low field region of the loops, **b** FC(black)/ZFC(red) magnetization curves acquired at 50 Oe and **c** FC magnetization curves measured in different fields.

## Role of H<sub>2</sub>O and other synthetic parameters in the hollowing mechanism

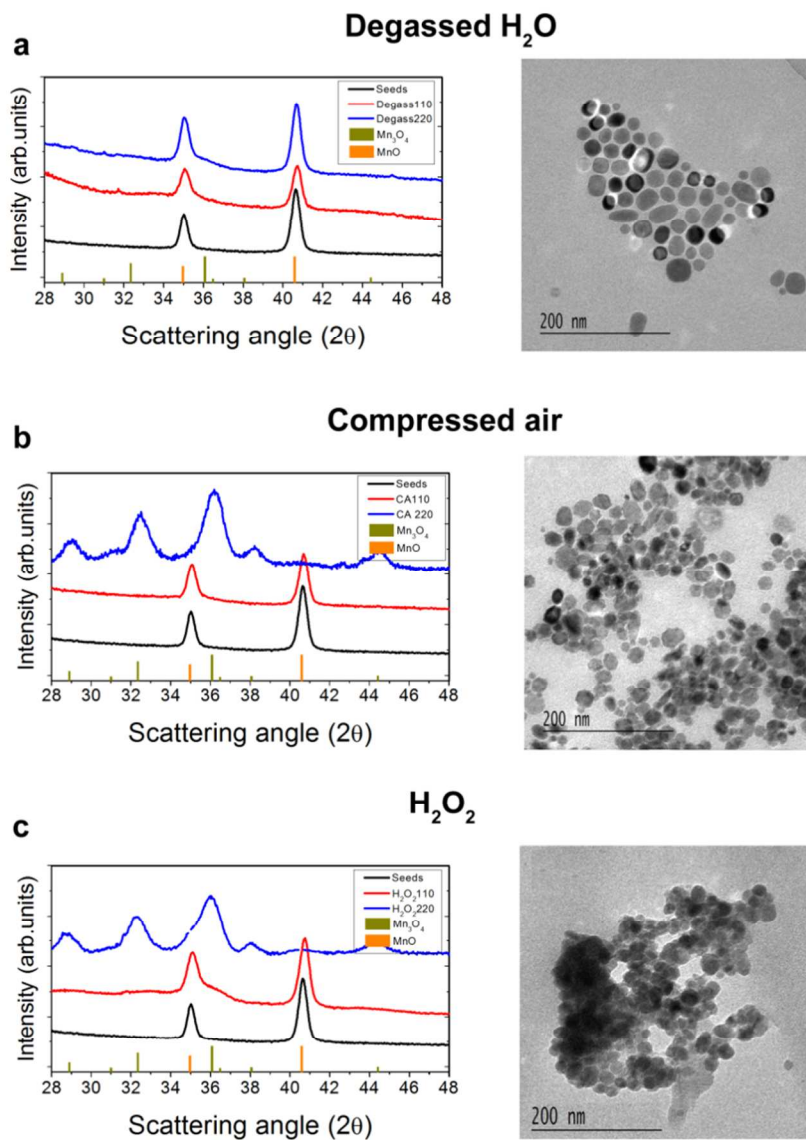


**Figure S3.** XRD patterns and TEM images for samples annealed with **a** deoxygenated (Argon-bubbled) H<sub>2</sub>O, **b** compressed air and **c** H<sub>2</sub>O<sub>2</sub>.

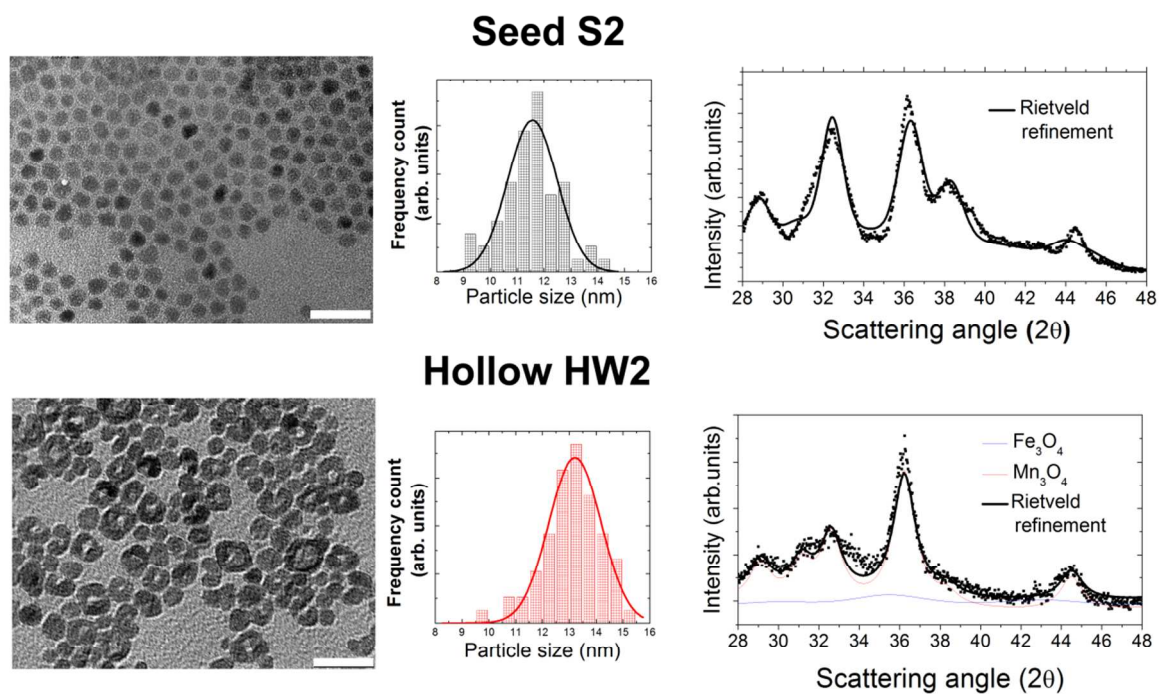


**Figure S4.** TEM images, particle size histograms and XRD patterns for the pure Mn<sub>3</sub>O<sub>4</sub> nanoparticles, **S2**, and for the **HW2** nanoparticles. Scale bars correspond to 20 nm.

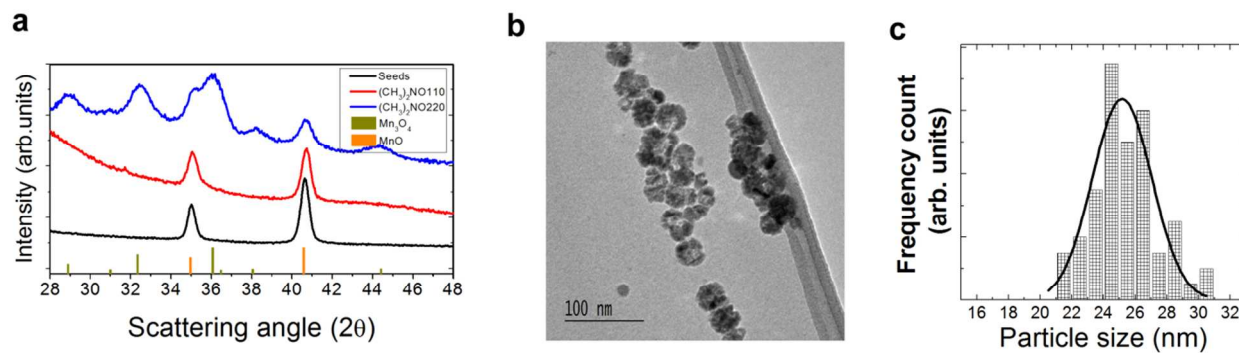


**Figure S5.** **a** XRD patterns for samples annealed with (CH<sub>3</sub>)<sub>3</sub>NO at 110 and 220 °C, **b** TEM images of the hollow **HW3** nanoparticles and **c** particle size histogram.

### **Effect of oleic acid/oleylamine in the hollowing process**

The *effect of oleic acid/oleylamine in the reaction* was tested in order to confirm the galvanic replacement as the main hollowing mechanism, and to discard any acid etching mediated process. Core-shell MnO/Mn<sub>3</sub>O<sub>4</sub> and pure Mn<sub>3</sub>O<sub>4</sub> nanoparticles were solved in dibenzyl ether and heated up to 220 °C and a mixture of oleic acid/oleylamine was injected (without the presence of the iron precursor), since it has been reported that organic acids can hollow oxide particles through acid etching<sup>2</sup> at high temperatures. However, as can be seen in Figure S6a,b, the resulting nanoparticles do not show the appearance of the voids characteristic of hollow structures. Therefore, etching processes can be discarded to play a major role in the hollowing process in the Mn<sub>3</sub>O<sub>4</sub>-Fe<sub>3</sub>O<sub>4</sub> systems, leaving galvanic replacement as the most probable responsible mechanism in the formation of hollow nanoparticles.

Finally to study the effect of the bonding strength of the capping ligands of the seeds on the kinetics of the formation of the heterostructures,<sup>3</sup> the capping ligand of pure Mn<sub>3</sub>O<sub>4</sub> seed nanoparticles was exchanged from oleylamine to oleic acid, since oleic acid has a much stronger affinity to Mn atoms. However, the hollowing process due to the iron deposition is not affected by the change of ligand (see Figure S6c). Therefore, it can be concluded that the kinetics of the galvanic replacement is not strongly modified by the higher bonding strength between surface manganese atoms and the carboxylic group of the oleic acid. Indeed, here the affinities of NH<sub>2</sub> and COOH groups for the oxides are similar and low, while the contrary is observed in the case of AgAu nanoparticles where the affinity of NH<sub>2</sub> groups is much higher than that of COOH functional groups.<sup>3</sup>

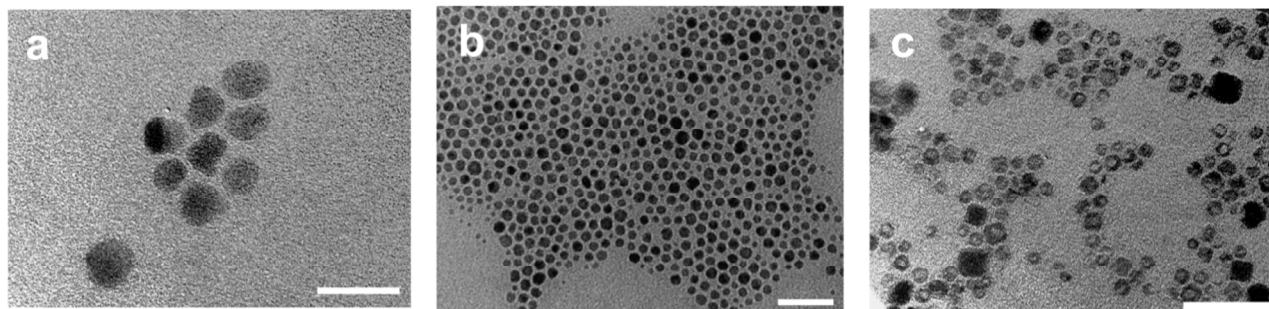


**Figure S6.** TEM images for **a** core/shell MnO/Mn<sub>3</sub>O<sub>4</sub> and **b** pure Mn<sub>3</sub>O<sub>4</sub> nanoparticles heated and digested after the injection of a mixture of oleic acid/oleylamine; and **c** pure Mn<sub>3</sub>O<sub>4</sub> nanoparticles oleic acid capping agent exchange after seeded-growth iron deposition (Scale bars 50 nm).

### Capping ligand exchange

40 mg of as-prepared **S2** nanoparticles were dissolved in a mixture of 20 mL of 1-octadecene and 5 mL of oleic acid, degassed and heated up to 80 °C for 24 hours. The nanoparticles were washed by several cycles of coagulation with ethanol, centrifugation at 5000 rpm, disposal of supernatant solution and re-dispersion in hexane.

The exchange of the capping ligand for sample **S2** has been corroborated by the analysis of the respective Fourier transform infrared (FTIR) spectra. Figure S8 shows characteristic C-H aliphatic symmetric and asymmetric stretching vibrations in the range of 2840-2950 cm<sup>-1</sup> typical for hydrocarbon chains. In particular as-prepared **S2** nanoparticles with the band for N-H stretch at 3425 cm<sup>-1</sup>, indicate the presence of the oleylamine as a capping ligand. Conversely, after ligand exchange reaction with oleic acid absorption bands associated to the N-H stretch disappear and an extra band related to the C=O stretching is observed at 1700 cm<sup>-1</sup> giving

evidences of the complete exchange of oleylamine by oleic acid as it is expected due to the higher affinity of oleic acid for manganese ions than oleylamine.<sup>3</sup>

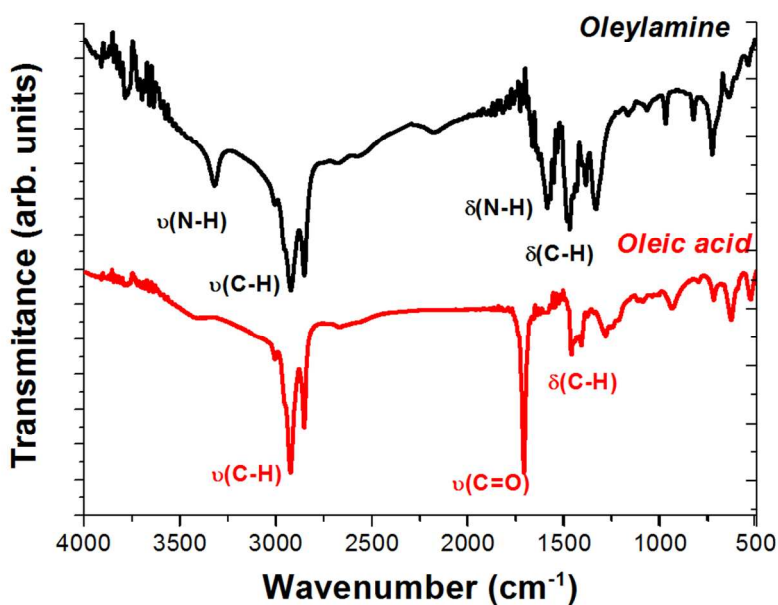


**Figure S7.** FTIR spectra for sample S2 capped with oleylamine and oleic acid, respectively.

### Fe precursor reduction

It should be pointed out that in our case the iron precursor is in a trivalent oxidation state which is then reduced to  $\text{Fe}^{2+}$  by the generated reducing agents (i.e., CO and  $\text{H}_2$ )<sup>4-6</sup> in the degassed environment during the decomposition of the organic chain of the metal precursor and free surfactants<sup>5</sup>, leading to the kickoff of the galvanic replacement.

## REFERENCES

- (1) Yedra, L.; Xuriguera, E.; Estrader, M.; López-Ortega, A.; Baró, M. D.; Nogués, J.; Roldan, M.; Varela, M.; Estradé, S.; Peiró, F. Oxide Wizard: An EELS Application to Characterize the White Lines of Transition Metal Edges. *Microsc. Microanal.* **2014**, *20*, 698–705.
- (2) An, K.; Kwon, S. G.; Park, M.; Na, H. Bin; Baik, S.-I.; Yu, J. H.; Kim, D.; Son, J. S.; Kim, Y. W.; Song, I. C.; Moon, W. K.; Park, H. M.; Hyeon, T. Synthesis of Uniform Hollow Oxide Nanoparticles through Nanoscale Acid Etching. *Nano Lett.* **2008**, *8*, 4252–4258.
- (3) Lu, X.; Tuan, H.-Y.; Chen, J.; Li, Z.-Y.; Korgel, B. A.; Xia, Y. Mechanistic Studies on the Galvanic Replacement Reaction between Multiply Twinned Particles of Ag and H<sub>2</sub>AuCl<sub>4</sub> in an Organic Medium. *J. Am. Chem. Soc.* **2007**, *129*, 1733–1742.
- (4) Estrader, M.; López-Ortega, A.; Golosovsky, I. V.; Estradé, S.; Roca, A. G.; Salazar-Alvarez, G.; López-Conesa, L.; Tobia, D.; Winkler, E.; Ardisson, J. D.; Macedo, W. A. A.; Morphis, A.; Vasilakaki, M.; Trohidou, K. N.; Gukasov, A.; Mirebeau, I.; Makarova, O. L.; Zysler, R. D.; Peiró, F.; Baró, M. D.; Bergström, L.; Nogués, J. Origin of the Large Dispersion of Magnetic Properties in Nanostructured Oxides: Fe<sub>3</sub>O<sub>4</sub>/Fe<sub>3</sub>O<sub>4</sub> Nanoparticles as a Case Study. *Nanoscale* **2015**, *7*, 3002–3015.
- (5) Bronstein, L. M.; Huang, X.; Retrum, J.; Schmucker, A.; Pink, M.; Stein, B. D.; Dragnea, B. Influence of Iron Oleate Complex Structure on Iron Oxide Nanoparticle Formation. *Chem. Mater.* **2007**, *19*, 3624–3632.
- (6) Lottini, E.; López-Ortega, A.; Bertoni, G.; Turner, S.; Meledina, M.; Tendeloo, G. Van; de Julián Fernández, C.; Sangregorio, C. Strongly Exchange Coupled Core|shell Nanoparticles with High Magnetic Anisotropy: A Strategy towards Rare Earth -Free Permanent Magnets. *Chem. Mater.* **2016**, *28*, 4214–4222.